Available online at www.sciencedirect.com
SCIENCE DIRECT®
Journal of Computational Physics 201 (2004) 586–600
JOURNAL OF COMPUTATIONAL PHYSICS
www.elsevier.com/locate/jcp

High order WENO schemes: investigations on non-uniform convergence for MHD Riemann problems

M. Torrilhon [a,*], D.S. Balsara [b]

[a] *Seminar for Applied Mathematics, ETH Zentrum, CH-8092 Zurich, Switzerland*
[b] *Department of Physics, University of Notre Dame, Notre Dame, IN 46556-5670, USA*

Received 17 March 2004; received in revised form 15 June 2004; accepted 17 June 2004
Available online 13 August 2004

Abstract

Detailed empirical error and convergence studies for high order weighted essentially non-oscillatory (WENO) schemes are presented in the case of special magnetohydrodynamic Riemann problems. The results supplement the results for standard high resolution finite volume schemes given in [M. Torrilhon, Non-uniform convergence of finite-volume-schemes for Riemann problems of ideal magnetohydrodynamics, J. Comput. Phys. 192 (2003) 73–94]. The special Riemann problems are based on initial conditions that are close to initial conditions which admit non-unique solutions. Like the standard methods the WENO schemes investigated in this paper exhibit a strongly non-uniform convergence behavior with initial convergence to a wrong solution (pseudo-convergence). However, the cancelation of the pseudo-convergence occurs at coarser grids for higher order methods.

MSC: 65M12; 76W05
Keywords: Hyperbolic partial differential equations; Magnetohydrodynamics; Riemann problem; Higher order methods; WENO schemes

1. Introduction

The equations of ideal magnetohydrodynamics (MHD) build a hyperbolic system of partial differential equations. The accurate numerical solution of the system becomes relevant in the description of

* Corresponding author.
E-mail addresses: manuel@math.ethz.ch (M. Torrilhon), dbalsara@nd.edu (D.S. Balsara).

0021-9991/$ - see front matter © 2004 Elsevier Inc. All rights reserved.
doi:10.1016/j.jcp.2004.06.015

non-dissipative plasma flows, see [16] or [18]. In this paper, we will consider Riemann problems for the system of ideal MHD in order to test the convergence behavior of higher order finite volume schemes. Furthermore, the results will be put in context against a standard scheme to allow a direct comparison.

Only recently, a special class of Riemann problems has been proposed in [27] for the testing of MHD schemes. Several standard high resolution methods, like Roe-type or central schemes, have been tested and all schemes exhibit a pathological, non-uniform convergence behavior, see [27]. Since the high resolution methods have been exclusively second order, the question arises whether higher order schemes show a different performance. This investigation is the concern of the present paper. In many aspects this paper must be seen as supplement of [27]. We skip a detailed discussion of the test problems and concentrate on the presentation of the empirical error studies.

The non-uniform convergence is only present for specially chosen Riemann problems which, nevertheless, have physical relevance. The pathological behavior is briefly described as follows: up to a certain number of grid points the numerical solution seems to converge to a wrong solution in which irregular wave patterns exist. The error with respect to the true solution does not decrease for several grid refinements. Instead parts of the solution may be shown to converge to irregular wave patterns which are not present in the true solution. However, after a considerable increase of grid cells, convergence to the true solution is established and the numerical scheme converges to the true solution. The initial convergence appears as pseudo-convergence.

The special Riemann problems are constructed in [27] using the non-classical hyperbolic properties of the MHD system. The system is non-strictly hyperbolic with non-convex flux function and the characteristic fields are no longer either genuinely non-linear or linearly degenerate. By virtue of this, the MHD system may admit non-classical (non-regular) waves, like compound waves and overcompressive shocks, so-called *intermediate* waves.

The constitution and relevance of intermediate waves is still discussed in the literature. Early work in this area was presented in [11,12]. In [20,21] a non-linear stability analysis is conducted and the intermediate waves have been found to be conditionally stable, but only when dissipation is present in the system. These waves have also been observed in 2d and 3d simulations, see [7–9]. However, it has also been argued against intermediate waves in [10].

The existence of these waves lead to non-unique solutions of certain Riemann problems, see e.g. [4,18,26]. The initial conditions which admit non-unique solutions can be shown to form a closed set [26]. Hence, for a non-unique problem there are initial conditions nearby which have only one, unique solution. The special Riemann problems constructed in [27] and used in the following are chosen in such a way. They admit a unique solution, but this solution lies in the vicinity of a non-unique solution. The non-uniform convergence behavior may be interpreted as interference of the solution in a regular domain with a non-unique solution which is nearby. In this paper, we use two of such *almost non-unique* Riemann problems. One is almost coplanar, and the other one is formulated in a non-planar setting. Both problems may also be found in [27]. Basically, the phenomena of non-uniform convergence has to be corrected by reducing the numerical diffusion. Usually, convergence problems like entropy glitches or occurrences of negative densities can be remedied by adding numerical diffusion. However, here the background is a non-continuous limit of the viscosity solution and the viscosity distracts the numerical solution from the ideal solution path.

The high order schemes tested in this paper stem from the class of weighted essentially non-oscillatory schemes as described in [19,15,14,1]. We choose a fifth and ninth order implementation. See Section 3.1 for more details of the methods. Basically, all higher order methods show the same non-uniform convergence as the lower order methods in [27]. This is in agreement with the conjecture in [27] that any diffusive numerical method will show this behavior to some extent. However, the higher order schemes exhibit some improvement concerning the cancellation of the pseudo-convergence. Also, the true convergence is faster in the case of higher order schemes. We also calculate the test problems

with time integrations of different order and demonstrate that the influence of the time integration seems to be negligible. In order to allow direct comparison to the results of [27] we use the same definition of the error and also present the error results of a standard Roe-type method.

The higher order methods do not entirely overcome the problem of non-uniform convergence though they do help one in achieving convergence to the true solution on coarser meshes. The main reason is that these methods do not reduce the numerical diffusion close to shocks due to the limiting procedure. A possible solution could be to use the ideas of [22], where a model system is investigated. The authors of [22] propose to build the numerical method upon a special Roe-solver whose averaging respects the rotational character of the magnetic field. Such a Riemann solver would help in one-dimensional problems but its use for multi-dimensional problems is less clear. Another possible solution that is perhaps more promising for multi-dimensional problems is to use divergence-free adaptive mesh refinement [2,3] to increase the mesh resolution in the vicinity of intermediate waves. Yet a third possible solution is to find schemes that have intrinsically lower errors on smaller meshes. The application of these ideas to the MHD system remains a topic for future work.

The paper is organized as follows: in Section 2 we recall the one-dimensional MHD equations and discuss the possible non-uniqueness and non-uniform convergence behavior. At the end of Section 2 the test problems are presented. In the beginning of Section 3 we introduce the higher order schemes used in this paper. Afterwards the error plots for the different methods and time integrations are discussed and compared to the results of the Roe-type scheme. The paper closes with a short conclusion.

2. Almost non-unique MHD Riemann problems

2.1. MHD equations

The variables of ideal magnetohydrodynamics are the fields of density ρ, flow velocity $\mathbf{v}$, magnetic flux density $\mathbf{B}$ and total energy E. In one-dimensional processes the vectorial variables $\mathbf{v}$ and $\mathbf{B}$ are split into their scalar normal components, v_n and B_n, in the direction of the space variable and the two-dimensional transversal parts, $\mathbf{v}_\mathrm{t}$ and $\mathbf{B}_\mathrm{t}$. If x is the space direction, we have

$$\mathbf{B} = (B_x, B_y, B_z) = (B_\mathrm{n}, \mathbf{B}_\mathrm{t}) \quad \text{and} \quad \mathbf{v} = (v_x, v_y, v_z) = (v_\mathrm{n}, \mathbf{v}_\mathrm{t}). \tag{1}$$

The amplitude of $\mathbf{B}_\mathrm{t}$ will be denoted by

$$B_\mathrm{t} = \|\mathbf{B}_\mathrm{t}\|. \tag{2}$$

Due to the divergence condition which has to be imposed on the magnetic field, the normal component B_n has to be constant in space in one-dimensional processes. The remaining seven fields

$$u = (\rho, v_\mathrm{n}, \mathbf{v}_\mathrm{t}, \mathbf{B}_\mathrm{t}, E), \tag{3}$$

build the set of variables for one-dimensional MHD. We consider only ideal gases and the total energy will be substituted by the pressure, which is related to E by

$$E = \frac{1}{\gamma - 1} p + \frac{1}{2}\rho v_\mathrm{n}^2 + \frac{1}{2}\rho \mathbf{v}_\mathrm{t}^2 + \frac{1}{2}\mathbf{B}^2. \tag{4}$$

Throughout the calculations of this paper the adiabatic constant γ is set to be $\gamma = 5/3$.

The one-dimensional MHD equations read:

$$\begin{aligned}
&\partial_t \rho + \partial_x(\rho v_\mathrm{n}) = 0,\\
&\partial_t \rho v_\mathrm{n} + \partial_x(\rho v_\mathrm{n}^2 + p + \tfrac{1}{2}\mathbf{B}_\mathrm{t}^2) = 0,\\
&\partial_t \rho \mathbf{v}_\mathrm{t} + \partial_x(\rho v_\mathrm{n}\mathbf{v}_\mathrm{t} - B_\mathrm{n}\mathbf{B}_\mathrm{t}) = 0,\\
&\partial_t \mathbf{B}_\mathrm{t} + \partial_x(v_\mathrm{n}\mathbf{B}_\mathrm{t} - B_\mathrm{n}\mathbf{v}_\mathrm{t}) = 0,\\
&\partial_t E + \partial_x(E + p + \tfrac{1}{2}\mathbf{B}^2)v_\mathrm{n} - (B_\mathrm{n}\mathbf{B}_\mathrm{t}\cdot\mathbf{v}_\mathrm{t}) = 0.
\end{aligned} \tag{5}$$

The equation for the normal component of the magnetic flux density reduces to the statement that B_n is also constant in time. Thus, the normal field B_n is considered only as a parameter.

We recall that the system (5) is hyperbolic and has the characteristic velocities

$$\begin{aligned}
&\lambda_1 = v - c_\mathrm{f}, \quad \lambda_2 = v - c_\mathrm{A}, \quad \lambda_3 = v - c_\mathrm{s},\\
&\lambda_4 = v,\\
&\lambda_5 = v + c_\mathrm{s}, \quad \lambda_6 = v + c_\mathrm{A}, \quad \lambda_7 = v + c_\mathrm{f},
\end{aligned} \tag{6}$$

which are formed using the fast and slow magnetoacustic velocities $c_{\mathrm{f,s}}$, and the Alfven velocity c_A, see e.g. [13,16] or [18]. Since the eigenvalues may coincide at special points in the flow, the system (5) is only *non-strictly* hyperbolic.

2.2. The general Riemann problem

In a Riemann problem the system (5) is furnished with discontinuous initial conditions in the form

$$u(x, t=0) = \begin{cases} u^{(1)} & x < 0,\\ u^{(0)} & x > 0. \end{cases} \tag{7}$$

As mentioned above the normal magnetic field B_n has to be constant

$$B_\mathrm{n}^{(0)} = B_\mathrm{n}^{(1)} = B_\mathrm{n}, \tag{8}$$

and will be prescribed only as a parameter additionally to the initial conditions (7). The transverse field $\mathbf{B}_\mathrm{t}$, however, may vary from state 0 to state 1. In Fig. 1, we show general initial conditions for the

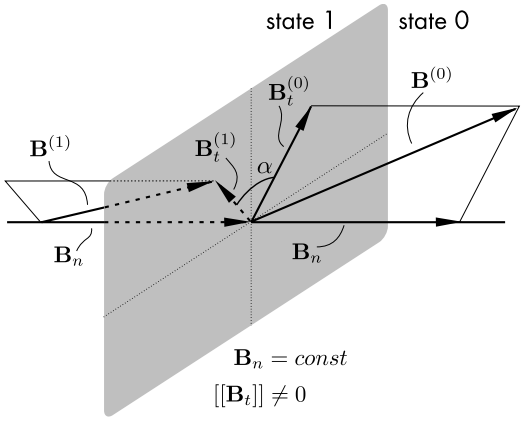

Fig. 1. The initial conditions of a MHD Riemann problem are separated into the constant states 0 and 1. Due to the divergence constraint the normal component of the magnetic field is not allowed to differ in both states. The transversal part may have different amplitudes as well as a twist angle α.

magnetic flux density. The absolute value as well as the direction of $\mathbf{B}_t$ may be different in both half-spaces. The initial twist angle of the planes of the magnetic fields is denoted by α. We use the following terminology: whenever the angle α is not an integer multiple of π the initial conditions are called *non-planar*. In a non-planar Riemann problem the magnetic fields in state 0 and 1 together with the direction of the space variable define different planes. In the case of α being a integer multiple of π the initial conditions are called *planar*. In the planar case, we distinguish between magnetic field vectors pointing in the same ($\alpha = 0$) or in opposite directions ($\alpha = \pi$). The case $\alpha = \pi$, where the magnetic field vectors are anti-parallel is called *coplanar*.

In the general case, the solution of a Riemann problem (7) for the MHD system is governed by seven waves, either discontinuities or rarefaction fans. Each wave is associated with a characteristic velocity in the following way:

$$v \pm c_f : \text{fast shock/rarefaction to the right/left}, \tag{9}$$

$$v \pm c_A : \text{rotational discontinuity to the right/left}, \tag{10}$$

$$v \pm c_s : \text{slow shock/rarefaction to the right/left}, \tag{11}$$

$$v : \text{contact discontinuity}. \tag{12}$$

The contact and rotational discontinuities are linear waves.

Most of the waves possible in a MHD Riemann problem form Lax shocks, linear waves or usual rarefaction waves, so-called regular waves. However, due to its non-strict hyperbolicity and non-convex flux function the MHD system admits several irregular waves, like overcompressive shocks, so-called intermediate waves, and compound waves. These irregular shock waves satisfy the entropy condition but more characteristics impinge on the shock than in Lax shocks (over-compressive shock). In a compound wave a rarefaction wave is directly attached to a marginally over-compressive shock.

2.3. Non-uniqueness

In [26] it has been argued that any MHD Riemann problem has at least one solution consisting only of regular waves. Only for certain critical choices of initial conditions the Riemann problem admits an additional solution with one or more intermediate waves. This makes the solution of the Riemann problem non-unique. In order to distinguish both possible solutions we speak of an *r-solution* in the case of the solution containing only regular waves and otherwise of a *c-solution* for the solution containing any non-regular waves like, for instance, compound waves.

A common feature of the non-unique solutions is the presence of a π-rotational wave in the r-solution which rotates the transverse magnetic field by an angle of π, i.e., it simply changes the sign of $\mathbf{B}_t$. In the c-solution this rotational wave is substituted by a wave pattern built by an intermediate wave which changes the sign of $\mathbf{B}_t$ as well. A π-rotational wave occurs, for instance, in the r-solution of a coplanar Riemann problem and the corresponding c-solution has been observed in [5]. The non-uniqueness was discussed in [4,6]. However, there exist also non-planar Riemann problems which admit π-rotational waves and in [26] it turned out that all these Riemann problems possess a non-unique solution.

The critical choices form a hypersurface with one codimension in the space of the initial conditions. Hence, there are initial conditions having only unique regular solutions arbitrarily close to a critical choice. The appearance of the non-uniqueness is also discussed in [27] in more detail.

2.4. Non-uniform convergence

The existence of non-unique solutions poses considerable problems to numerical methods for MHD. Remarkably, these problems are not restricted to the initial conditions which directly admit non-unique solutions. Convergence problems also occur in the case of solutions for initial conditions which are *close to* initial data with non-unique solutions.

In [27] non-uniform convergence has been reported to be present for a broad class of classical finite volume schemes for magnetohydrodynamics. Qualitatively, the behavior of the methods is described as follows. Up to a certain resolution of the grid the methods appear not to converge to the true (unique) solution of the problem considered. Instead, considerable convergence rates can be observed with respect to a c-solution of a nearby non-unique problem. This pseudo-convergence stops abruptly at a certain grid resolution and convergence to the true solution is established.

This behavior typically occurs for MHD Riemann problems with initial conditions which form a small perturbation of non-unique initial data. It is present, e.g. for almost coplanar initial conditions. In [27] two classes of initial conditions are given which allow detailed investigations of the convergence behavior of MHD schemes. The following two Riemann problems are taken from these classes.

2.5. Coplanar test problem

A possible coplanar Riemann problem is given by the initial conditions (7) with

$$\begin{aligned}\left(\rho_1, v_{\mathrm{n}}^{(1)}, \mathbf{v}_{\mathrm{t}}^{(1)}, B_{\mathrm{n}}, \mathbf{B}_{\mathrm{t}}^{(1)}, p_1\right) &= \left(1, 0, \mathbf{0}, 1, \begin{pmatrix}1\\0\end{pmatrix}, 1\right),\\ \left(\rho_0, v_{\mathrm{n}}^{(0)}, \mathbf{v}_{\mathrm{t}}^{(0)}, B_{\mathrm{n}}, \mathbf{B}_{\mathrm{t}}^{(0)}, p_0\right) &= \left(0.2, 0, \mathbf{0}, 1, \begin{pmatrix}\cos\alpha\\ \sin\alpha\end{pmatrix}, 0.2\right),\end{aligned} \tag{13}$$

if the twist angle is set to be $\alpha = \pi$. The velocity vanishes initially and density and pressure have values from a classical shock tube problem. State 1 (state 0) is the high (low) pressure domain. This Riemann problem is non-unique and admits two solutions, an r-solution and a c-solution.

In order to study the non-uniform convergence we consider the case

$$\alpha = 3.0. \tag{14}$$

In that case the initial conditions (13) are *almost* coplanar, and admit only one r-solution which is unique, see [26]. In the wave patterns of the solution arises a fast rarefaction wave and a slow shock wave at both sides of the contact discontinuity. Additionally, a strong rotational wave with an angle of almost π propagates to the left and a weak rotational wave with a very small angle propagates to the right.

The solution for the density and magnetic flux density component B_y is displayed and discussed in Section 3.2.

2.6. Non-planar test problem

Non-planar initial conditions that admit a non-unique solution are given by

$$\begin{aligned}\left(\rho_1, v_{\mathrm{n}}^{(1)}, \mathbf{v}_{\mathrm{t}}^{(1)}, B_{\mathrm{n}}, \mathbf{B}_{\mathrm{t}}^{(1)}, p_1\right) &= \left(1.7, 0, \mathbf{0}, 1.1, \begin{pmatrix}1\\0\end{pmatrix}, 1.7\right),\\ \left(\rho_0, v_{\mathrm{n}}^{(0)}, \mathbf{v}_{\mathrm{t}}^{(0)}, B_{\mathrm{n}}, \mathbf{B}_{\mathrm{t}}^{(0)}, p_0\right) &= \left(0.2, 0, \begin{pmatrix}0\\1.4968909\end{pmatrix}, 1.1, \begin{pmatrix}\cos\beta\\ \sin\beta\end{pmatrix}, 0.2\right),\end{aligned} \tag{15}$$

with an initial twist angle $\beta = \beta^* = 2.4$, see [26,27]. The possibility to have a non-planar c-solution is realized by an appropriate choice of the initial transversal velocity $\mathbf{v}_t$. The initial values for density, pressure and normal magnetic field are slightly changed in comparison to the coplanar case (13).

If we choose $\beta \neq \beta^*$, the Riemann problems becomes unique. In this paper, we consider the case

$$\beta = 2.3. \tag{16}$$

The solution contains two strong rotational waves one of which has an angle of almost π. If the initial twist angle approaches β^* this waves turns into a π-rotation which is substituted by an intermediate wave in the possible c-solution.

Both Riemann problems (13) and (15) with (14)/(16) lead to non-uniform convergence of finite-volume-schemes, see [27]. In the next section, we will study the behavior of high order WENO methods applied to these problems.

3. Results

In this section, we shall use the notation

problem 1 : (13) with (14),

problem 2 : (15) with (16),

for the coplanar and non-planar test problem. All results for both problems have been obtained in the computational domain

$$x \in [1, 1.5], \tag{17}$$

with uniform mesh and the end time was chosen to be

$$t_{\text{end}} = 0.4. \tag{18}$$

3.1. Numerical methods

We consider two representatives of the class of weighted essentially non-oscillatory schemes as described in [15,1,14], namely the WENO schemes with $r = 3$ and $r = 5$, denoted by 3WENO and 5WENO. Both schemes exhibit $(2r - 1)$th order in space for smooth solutions. We used the Roe-Friedrichs variant of the WENO schemes described above because that choice is known to produce the crispest representation of discontinuities with WENO schemes, as shown in [24]. The Roe-Friedrichs scheme requires a decomposition into characteristic variables for which we used the eigenstructure of the MHD equations as catalogued in [23]. Additionally, we use the Monotonicity Preserving (MP) extensions of these two WENO schemes as described in [1]. The extended schemes have improved monotonicity properties which endows them with the greater stability that is needed for more stringent hydrodynamical and MHD problems. They are denoted by 3MPWENO and 5MPWENO. As with the base schemes, these schemes are fifth and ninth order in space, respectively, for very smooth problems.

All simulations were done with the temporally third-order accurate, TVD-preserving Runge-Kutta time-stepping method from [24] and many of the simulations were repeated with a fourth-order accurate Runge-Kutta time-stepping method. The influence of the time integration is discussed in Section 3.3. In a numerical scheme, time and space error may at times be swapped, thus the overall order of the schemes might be limited by the temporal accuracy. The use of fourth-order accurate time-integration, therefore, allows us to ensure that our results are formally at least fourth-order accurate in both space and time. Since

all problems considered in the following contain discontinuous solutions, the order of convergence will be bounded by unity in any case. In calculations with the WENO schemes the maximal Courant number was 0.4.

The schemes are applied to both test problems at increasing numbers of grid cells. The results are compared to the exact solution obtained with the Riemann solver described in [25] (solutions are also given in [27]). The L^1-error is calculated using

$$\mathrm{err}_N = \sum_{i=1}^{N} \Delta x \left| \psi_i^{(\mathrm{num})} - \psi^{(\mathrm{ex})}(x_i) \right|, \tag{19}$$

where ψ is the density or a component of the magnetic flux density. The empirical order of convergence follows from

$$\mathrm{EOC}_{N_1,N_2} = \frac{\log\left(\frac{\mathrm{err}_{N_1}}{\mathrm{err}_{N_2}}\right)}{\log\left(\frac{N_2}{N_1}\right)}, \tag{20}$$

if two errors of successively refined solutions with N_1 and N_2 grid points are given.

In order to compare the results to the error plots in [27], we also present the results of a calculation with a standard high resolution method. Therefore, we choose a Godunov-type scheme with Roe solver and linear reconstruction. The reconstruction is limited using the minmod limiter and the maximal Courant number was 0.9. For smooth solution this method is second order in space and time. Note, that the non-uniform convergence behavior is not restricted to Roe-type schemes. In [27] it has been demonstrated for a broad set of high resolution methods.

In the following, we will only compare the error of the different methods and not the efficiency. Since we used totally different implementations for the Roe-type and WENO schemes, statements about running times are not comparable and therefore suppressed.

For hyperbolic equations with non-convex flux function it is known that the traditional Courant number may under-estimate the actual wave speed. This results in convergence problems in some cases, see [17]. In the case of MHD the Courant number is calculated from the eigenvalue of the fast characteristic family, which is not affected from the non-convexity, see [26]. The numerical simulations also appeared not to be sensitive to the chosen value of the maximal Courant number.

Before we present results for the empirical order of convergence we discuss the qualitative behavior of the solution.

3.2. Qualitative behavior

Qualitatively, all (MP)WENO schemes exhibit the same kind of non-uniform convergence as the standard schemes presented in [27]. Also, the kind of mismatch of the true solution is comparable. In this section, we present the results of the 3WENO scheme at a grid resolution $N = 800$ which can be directly compared to the results for a standard TVD scheme in [27].

The following plots are obtained by applying the 3WENO scheme with 800 grid cells ($\Delta x = 3.125 \times 10^{-3}$) to the almost coplanar Riemann problem (problem 1). In Fig. 2 the computed fields of density and magnetic field component B_y are shown with light boxes.

The true solution is plotted using a dashed line. Additionally, the c-solution of the nearby coplanar problem is plotted with a dotted line. Of course, this solution is not a solution to problem 1 since the coplanar problem has different left and right hand states, see enlargement in Fig. 3. The numerical solution in Fig. 2 nicely resolves the right going slow shock and rarefaction wave. In the negative half-space, however, the numerical solution fails to compute the rotational wave and the slow shock. Instead, the numerical solution

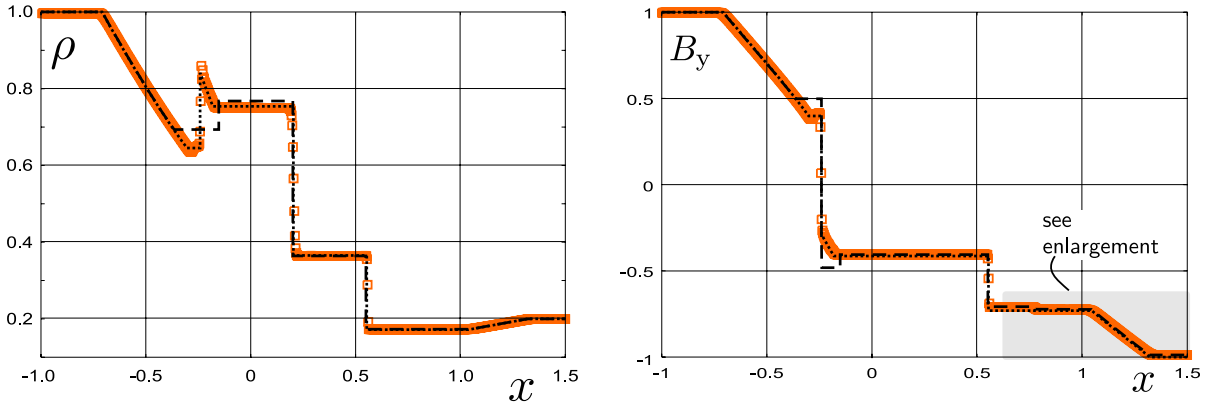

Fig. 2. Results of the 3WENO scheme for the density field and magnetic flux density component obtained with 800 grid cells in the case of problem 1. The numerical solution is shown with light boxes. The dashed line represents the exact solution. The dotted line shows the c-solution of the nearby co-planar problem. The numerical solution follows the compound wave pattern of the incorrect solution.

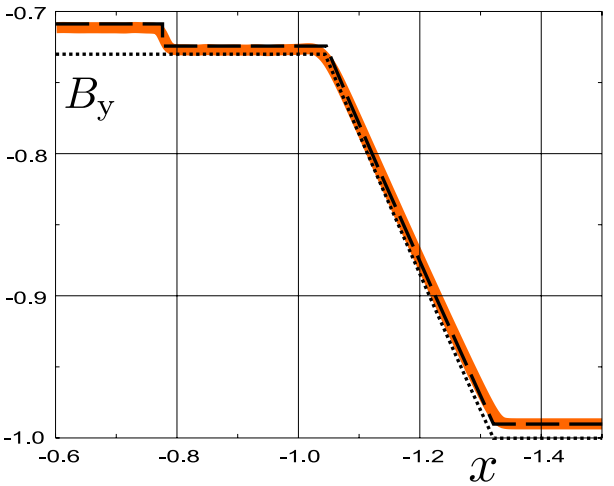

Fig. 3. A detailed view at the solution for the magnetic flux density as shown in Fig. 2. The c-solution of the coplanar problem (dotted), which seems to be approximated in Fig. 2, is not matched at the right boundary, since it differs in the value of B_y at state 0.

shows the pattern of the compound wave as it appears in the c-solution of the coplanar problem. Also, at the position $x = 0$ the density of the numerical solution rather matches the value of the c-solution. Hence, the numerical scheme seems to converge to a wrong solution, at least at the level of 800 grid cells.

Towards the right-hand side the numerical solution leaves the c-solution and follows the true solution, as can be seen in the detail plot of Fig. 3. It shows the field of the magnetic flux density component B_y in the interval [0.6,1.5].

If the grid is refined the compound wave pattern starts to break apart at a certain level of resolution. This behavior has been thoroughly discussed in [27] and we will not go into the details in this paper. With further refinement the density peak shrinks more and more and the shock of the true solution is very slowly recovered. Correspondingly, the wave pattern for the magnetic flux component B_y starts to approach the amplitude of the rotational wave. At last, convergence to the true solution is obtained. The entire convergence is non-uniform and the initial convergence to a wrong solution appeared as *pseudo-convergence*.

3.3. Empirical order of convergence

3.3.1. Third/fourth higher order time stepping

We calculated problem 1 with the 5MPWENO method using a third and a fourth order time integration. Table 1 shows the L^1-errors of the solution for B_y in the interval $[-0.5,0.0]$ for both time integrations. The first two and last two columns consider the error with respect to the true solution and to the wrong c-solution, respectively. As can be seen from the table the deviations of the error between the different time integrations are very small. Note that the table shows the logarithm (base 10) of the error and the deviations occur only in the third digit. The reason for the little difference between both time integrations lies in the spatial non-smoothness of the solution. The time integration would only show considerable influence if the solution was sufficiently smooth.

We conclude that the influence of the time integration is negligible for the present test problems. The calculations of the next sections use only the third order time integration. Since the 5(MP)WENO and 3(MP)WENO methods indeed give different results (see next section) the order of the space resolution is considered to give the main influence.

3.3.2. Problem 1

There is a main difference in the non-uniform convergence behavior between the (MP)WENO schemes and the standard TVD schemes in [27]: the pseudo-convergence cancels at coarser grid resolutions, hence the true solution is recovered on coarser grids. This can best be seen by plotting the errors for solutions at different grid resolutions.

Following the same procedure as in [27] for problem 1 only the interval $[-0.5, 0.0]$ is considered for the calculation of the error and only the error of the field of B_y is shown. The error is computed both with respect to the true solution and with respect to the c-solution of the coplanar problem. As mentioned already above, this c-solution is not an analytical solution for problem 1. Nevertheless, during the pseudo-convergence at coarse grids the numerical methods exhibit convergence to this wrong solution.

Figs. 4 and 5 display the L^1-error of numerical solutions for problem 1 obtained with the 3/5(MP)WENO schemes at several grid resolutions.

For comparison the errors of the Roe-type method are shown as well. Both figures show the same axes range. As general observation we remark that there is only little difference between the curves of the WENO and the MPWENO schemes.

Table 1
L^1-error study and empirical order of convergence for the 5MPWENO scheme with time integrations of third and fourth order

N	With respect to exact solution		With respect to c-solution	
	$\log(\mathrm{err}_N^{(3rd)})$	$\log(\mathrm{err}_N^{(4th)})$	$\log(\mathrm{err}_N^{(3rd)})$	$\log(\mathrm{err}_N^{(4th)})$
50	−1.56926	−1.56865	−1.34465	−1.34504
100	−1.79689	−1.79711	−1.46626	−1.46716
200	−2.03490	−2.03432	−1.56210	−1.56232
400	−2.24425	−2.24236	−1.62532	−1.62511
800	−2.36240	−2.36311	−1.67009	−1.67037
1200	−2.24148	−2.24138	−1.74165	−1.74170
1600	−2.10573	−2.10491	−1.81362	−1.81251
3000	−1.90871	−1.90881	−2.00868	−2.00859
5000	−1.82152	−1.82150	−2.18964	−2.18970
10,000	−1.75553	−1.75558	−2.44780	−2.44757
20,000	−1.72050	−1.72061	−2.71117	−2.71074

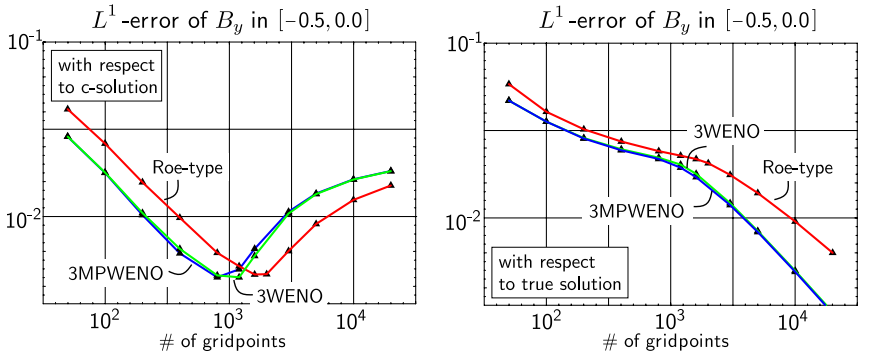

Fig. 4. L^1-errors of the magnetic flux density component B_y for problem 1, (13) with (14) calculated with the schemes 3WENO and 3MPWENO. The left plot shows the error calculated with respect to the c-solution of the coplanar problem. The right plot displays the error with respect to the true solution. Additionally, the error curve for the Roe-type scheme is displayed in both plots.

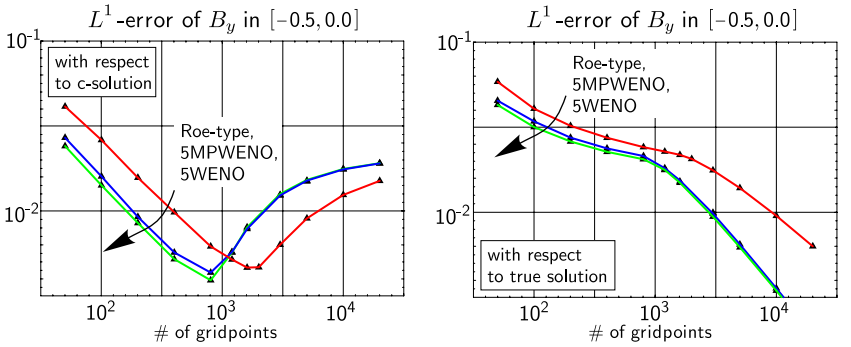

Fig. 5. L^1-errors of the magnetic flux density component B_y for problem 1, (13) with (14) calculated with the schemes 5WENO and 5MPWENO. The left plot shows the error calculated with respect to the c-solution of the coplanar problem. The right plot shows the error with respect to the true solution. Additionally, the error curve for the Roe-type scheme is displayed in both plots.

In both figures the left plot shows the error with respect to the c-solution. All curves in these plots come along with a distinct kink indicating the cancellation of the initial pseudo-convergence.

This kink is shifted towards coarser grids for the higher order schemes. For the Roe-type scheme convergence towards the true solution starts approximately at 1600 grid cells. In the case of 3(MP)WENO true convergence starts already at 1000 grid cells and the kink appears even earlier, at approximately 800 grid cells, for the 5(MP)WENO schemes.

Since the onset of true convergence is mainly driven by the amount of dissipation in the numerical schemes (see [27]), the present results for higher order schemes can be explained by the reduced dissipation in those methods. On the other hand all (MP)WENO schemes are reconstruction-based schemes. To obtain higher order these schemes are using data from larger and larger stencils. At some point the schemes use information whose influence for an update is rather questionable. Hence, we do not expect that ever higher order will be able to push the pseudo-convergence to coarser and coarser grids. Nevertheless, the earlier cancellation of pseudo-convergence is a clear advantage of the higher order (MP)WENO schemes.

The MPWENO schemes are constructed with somewhat more dissipation than the classical WENO methods. Nevertheless, this is not reflected in the present error plots. This is significant because it shows that as the order of accuracy is increased, the convergence to the true solution is accelerated for both

the WENO and the MPWENO schemes. It is also significant because it shows that the monotonicity preserving addition to the WENO schemes does not degrade their convergence to the true solution in any way.

The right-hand side of Figs. 4 and 5 display the error with respect to the true solution. In correspondence to the left hand side convergence is obtained only beyond a certain refinement. Once the true solution is captured by the numerical scheme and the pseudo-convergence has been overcome, the (MP)WENO schemes show a clearly faster convergence. A close look leads to the following final order of convergences

$$\begin{aligned} &\text{Roe-type : EOC } 0.6,\\ &3\text{(MP)WENO : EOC } 0.75,\\ &5\text{(MP)WENO : EOC } 0.85, \end{aligned} \tag{21}$$

based on the two highest grid resolutions. Hence, the higher order schemes converge faster also in the presence of shock waves. This acceleration may be explained with the better approximation of the shock speed in case of the higher order schemes. Note, that this acceleration is not present during the pseudo-convergence at coarse grids as can be read off the left plots.

The general comparison of the (MP)WENO and the Roe-type schemes shows also that the high order schemes mainly give the smaller error indicating a smaller error constant. However, this is true both during the unwanted pseudo-convergence and true convergence.

Finally, the error of B_y with respect to the c-solution in the left plots of Figs. 4 and 5 has the asymptotic value of 0.2×10^{-1}. This is the L^1-distance between the true solution and the c-solution in the interval $[-0.5, 0.0]$. The value may be calculated from the analytical solutions. The asymptotic value is approached faster in the case of the (MP)WENO schemes.

Furthermore, it is interesting to note that the minimal error with respect to the c-solution is approximately the same for all schemes. This is a systematic feature that we find in the next problem, too. At this minimal error the pseudo-convergence stops and the scheme starts to approximate the correct solution. The key quantity in this process is the amount of B_z which is built up in the intermediate wave, see [11,12,27]. The break-up is related to a critical amount of B_z which is reached if the numerical viscosity drops below a critical value. Whenever different schemes reach this critical viscosity, maybe at different resolutions, the solutions will be very similiar, since the numerical viscosity is similiar. Hence, the L^1-distance to the correct solution will be the similiar for these different schemes. See also [27] for more details.

Taken together, the results suggest that there is a minimum numerical viscosity, i.e. numerical error, that a scheme should reach before it starts displaying convergence to the correct solution. Since higher order schemes reach that viscosity on smaller numbers of mesh points, they converge to the true solution on smaller meshes.

However, the improvement is small in comparison with the extra work that is done in the higher order methods. These methods are designed to reduce the numerical error in smooth regions, but they switch to lower order in the vicinity of shock waves in order to avoid oszillations. This limits the reduction of numerical viscosity and, hence, the improvements concerning the pseudo-convergence.

3.3.3. Problem 2

The Riemann problem 2 given in (15) with (16) has the same theoretical background as problem 1: its solution is unique but the initial conditions are close to initial conditions that admit a non-unique solution. However, the initial conditions of problem 2 are given entirely in a non-planar setting. Thus, this problem overcomes the somewhat special situation of coplanar data. Nevertheless, the numerical schemes applied to problem 2 exhibit behavior that is entirely similar to problem 1. The qualitative behavior of the solution is similar to that shown in Section 3.2.

For the sake of possible comparison with the results in [27] we choose to display the L^1-error of the density field in the interval $[-0.375, 0.0]$. Figs. 6 and 7 are presented analogously to Figs. 4 and 5 in the section above. The c-solution is now given by the c-solution of the initial conditions (15) with $\beta = \beta^*$.

In the present case of problem 2 the cancellation of pseudo-convergence is less pronounced. However, we can draw the same conclusions from the plots as in the case of the results for problem 1. The true convergences arises clearly earlier for the higher order schemes, but the pseudo-convergence is still present. The convergence towards the c-solution stops at approximately 400 grid cells.

Furthermore, the final orders of convergence are given by

$$\begin{aligned} &\text{Roe-type} : \text{EOC } 0.5, \\ &\text{3(MP)WENO} : \text{EOC } 0.7, \\ &\text{5(MP)WENO} : \text{EOC } 0.8, \end{aligned} \tag{22}$$

based on the finest calculations. We can again identify the fact that the higher order schemes lead to accelerated convergence also in the case of discontinuous solutions.

Analogously to the case of problem 1 there is an asymptotic value of the error with respect to the c-solution. It corresponds to the L^1-distance between the true solution and the c-solution. For the error of the

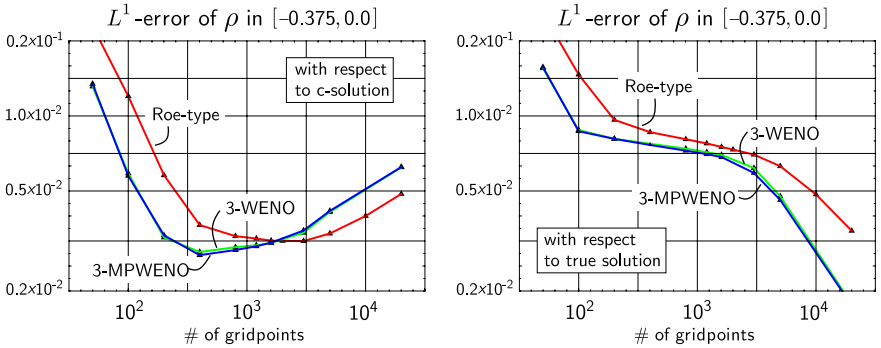

Fig. 6. Results for problem 2, (15) with (16) L^1-errors of the density calculated with the schemes 3WENO and 3MPWENO. The left plot shows the error calculated with respect to the c-solution of the nearby non-unique problem. The right plot shows the error with respect to the true solution. Additionally, the corresponding error curve for the Roe-type scheme is displayed in both plots.

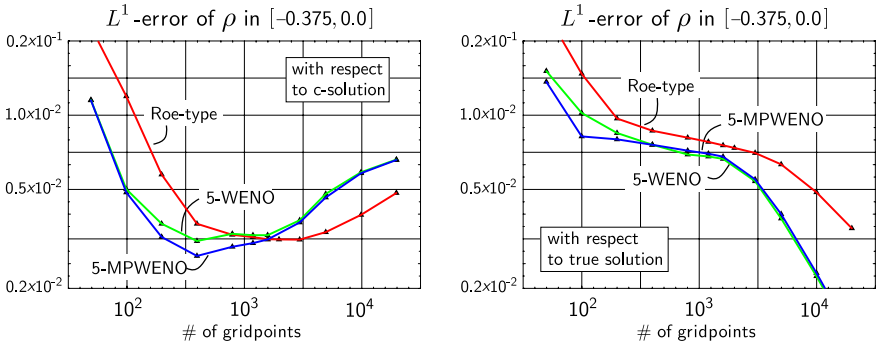

Fig. 7. Results for problem 2, (15) with (16) L^1-errors of the density calculated with the schemes 5WENO and 5MPWENO. The left plot shows the error calculated with respect to the c-solution of the nearby non-unique problem. The right plot presents the error with respect to the true solution. Additionally, the corresponding error curve for the Roe-type scheme is displayed in both plots.

density ρ in the present problem 2 it is given by approximately 0.7×10^{-2}. The curves in the left plots of Figs. 6 and 7 asymptotically approach that value.

4. Conclusions

In [27] non-uniform convergence behavior for *almost non-unique* Riemann problems of MHD has been demonstrated for several high resolution finite volume schemes. While the schemes in [27] have been only second order this paper supplements the investigation of higher order schemes applied to the special Riemann problems. Two methods from the WENO class and their monotonicity preserving counterparts (MPWENO) furnished as representatives for higher order schemes. The schemes exhibit fifth and ninth order spatial accuracy, respectively. The order of the time integration is found to have no influence due to the non-smooth solution. Our findings are:

- Basically, all higher order schemes investigated in this paper showed the same kind of non-uniform convergence as the plain second order methods.
- However, higher order methods establish the true convergence at coarser grids, i.e., the initial pseudo-convergence cancels faster.
- Furthermore, the true convergence is slightly faster with the (MP)WENO schemes.

The faster cancellation of pseudo-convergence of the higher order schemes can be understood as follows. In each problem where pseudo-convergence is displayed there is a minimum numerical viscosity past which the convergence reverts to the true convergence. This has also been discussed in [27]. Higher order schemes display smaller numerical viscosity than TVD schemes even on coarser meshes. As a result, they reach the true convergence on smaller meshes. However, this approach is limited, since the higher order methods are not designed to reduce the numerical viscosity directly at discontinuities. To stop pseudo-convergence reducing the diffusion around shock waves is the main issue, hence it will not pay off to go to ever higher order. In this paper the non-uniform convergence persists on coarser meshes. Pseudo-convergence is present up to grid sizes of $\Delta x \approx 5 \times 10^{-3}$, even for a ninth order WENO scheme.

This finding indicates that to obtain faster convergence to the true solution one needs numerical schemes with lower intrinsic error. In a subsequent paper we will show that this is the case for a class of divergence-free RKDG schemes that have been specially designed for MHD.

It is also possible to follow an *hp*-approach and to apply a sophisticated adaptation method that preserves the divergence-free structure of the magnetic field, see [2,3]. For one-dimensional problems one may want to incorporate a special Riemann solver which is specialized to resolved the rotational waves, as in [22] in the case of a model system.

Acknowledgments

Balsara wishes to acknowledge support via NSF Grants 005569-0001 and DMS-0204640.

References

[1] D.S. Balsara, C.-W. Shu, Monotonicity preserving weighted essentially non-oscillatory schemes with increasingly high order of accuracy, J. Comput. Phys. 160 (2000) 405–452.
[2] D.S. Balsara, Divergence-free adaptive mesh refinement for magnetohydrodynamics, J. Comput. Phys. 174 (2001) 614.

[3] D.S. Balsara, Second order accurate schemes for magnetohydrodynamics with divergence-free reconstruction, Astrophys. J. Suppl. 151 (2004) 149.
[4] A.A. Barmin, A.G. Kulikovskiy, N.V. Pogorelov, Shock-capturing approach and non-evolutionary solutions in magnetohydrodynamics, J. Comput. Phys. 126 (1996) 77.
[5] M. Brio, C.C. Wu, An upwind differencing scheme for the equations of ideal magnetohydrodynamics, J. Comput. Phys. 75 (1988) 400.
[6] W. Dai, P.R. Woodward, An approximate riemann solver for ideal magnetohydrodynamics, J. Comput. Phys. 111 (1994) 354.
[7] H. De Sterck, S. Poedts, Intermediate shocks in three-dimensional magnetohydrodynamic bow-shock flows with multiple interacting shock fronts, Phys. Rev. Lett. 84/24 (2000) 5524.
[8] H. De Sterck, S. Poedts, Disintegration and reformation of intermediate shock segments in three-dimensional MHD bow shock flows, J. Geophys. Res. 106 (2001).
[9] H. De Sterck, S. Poedts, Overcompressive shocks and compound shocks in 2D and 3D magnetohydrodynamic flows, in: Proceedings of the 8th International Conference on Hyperbolic Problems, International Series of Numerical Mathematics, vol. 141, 2001, p. 791.
[10] S.A.E.G. Falle, S.S. Komissarov, On the inadmissibility of non-evolutionary shocks, J. Plasma Phys. 65 (2001) 29.
[11] H. Freistuhler, E.B. Pitman, A numerical study of a rotationally degenerate hyperbolic system. part I. The riemann problem, J. Comput. Phys. 100 (1992) 306.
[12] H. Freistuhler, E.B. Pitman, A numerical study of a rotationally degenerate hyperbolic system. part II. The cauchy problem, SIAM J. Numer. Anal. 32 (1995) 741.
[13] A. Jeffrey, T. Taniuti, Non-linear Wave Propagation, Academic Press, New York, 1964.
[14] G.S. Jiang, C.-W. Shu, Efficient implementation of weighted ENO schemes, J. Comput. Phys. 126 (1996) 202–228.
[15] G.S. Jiang, C.C. Wu, A high-order WENO finite difference scheme for the equations of ideal magnetohydrodynamics, J. Comput. Phys. 150 (2) (1999) 561.
[16] L.D. Landau, E.M. Lifshitz, Electrodynamic of Continuous Media, Course in Theoretical Physics, vol. 8, Pergamon Press, Oxford, 1960.
[17] R.J. LeVeque, Finite Volume Methods for Hyperbolic Problems, Cambridge University Press, Cambridge, 2002.
[18] M.A. Liberman, A.L. Velikovich, Physics of Shock Waves in Gases and Plasmas, Springer Series in Electrophysics, vol. 19, Springer, Berlin, 1996.
[19] X.-D. Liu, S. Osher, T. Chan, Weighted essentially non-oscillatory schemes, J. Comput. Phys. 115 (1994) 200.
[20] R.S. Myong, P.L. Roe, Shock waves and rarefaction waves in magnetohydrodynamics. Part 1. A model system, J. Plasma Phys. 58 (3) (1997) 485.
[21] R.S. Myong, P.L. Roe, Shock waves and rarefaction waves in magnetohydrodynamics. Part 2. The MHD system, J. Plasma Phys. 58 (3) (1997) 521.
[22] R.S. Myong, P.L. Roe, On godunov-type schemes for magnetohydrodynamics, 1. A model system, J. Comput. Phys. 147 (1998) 545–567.
[23] P.L. Roe, D.S. Balsara, Notes on the eigensystem of magnetohydrodynamics, SIAM J. Num. Anal. 56 (1996) 57.
[24] C.-W. Shu, S. Osher, Efficient implementation of essentially non-oscillatory shock capturing schemes, J. Comput. Phys. 77 (1988) 439.
[25] M. Torrilhon, Exact Solver for Riemann Problems of Ideal Magnetohydrodynamics, Research Report 2002–06, Seminar for Applied Mathematics, ETH Zurich, 2002.
[26] M. Torrilhon, Uniqueness conditions for Riemann problems of ideal magnetohydrodynamics, J. Plasma Phys. 69 (3) (2003) 253.
[27] M. Torrilhon, Non-uniform convergence of finite-volume-schemes for Riemann problems of ideal magnetohydrodynamics, J. Comput. Phys. 192 (2003) 73–94.